Spin texturing in quantum wires with Rashba and Dresselhaus spin–orbit interactions and in-plane magnetic field

B Gisi[1,†], S Sakiroglu[2], and İ Sokmen[2]

[1] *Physics Department, Graduate School of Natural and Applied Sciences, Dokuz Eylül University, İzmir* 35390, *Turkey*
[2] *Physics Department, Faculty of Science, Dokuz Eylül University, İzmir* 35390, *Turkey*

(Received 21 July 2015; revised manuscript received 25 August 2015; published online 30 November 2015)

In this work, we investigate the effects of interplay of spin–orbit interaction and in-plane magnetic fields on the electronic structure and spin texturing of parabolically confined quantum wire. Numerical results reveal that the competing effects between Rashba and Dresselhaus spin–orbit interactions and the external magnetic field lead to a complicated energy spectrum. We find that the spin texturing owing to the coupling between subbands can be modified by the strength of spin–orbit couplings as well as the magnitude and the orientation angle of the external magnetic field.

Keywords: spin–orbit coupling, quantum wire, spin texture

PACS: 71.70.Ej, 75.70.Tj, 73.21.Hb, 85.75.–d **DOI:** 10.1088/1674-1056/25/1/017103

1. Introduction

Revolution and technological advance in semiconductor physics make it possible to fabricate high-precision nanostructured electronic devices. Exploring the physics of these low-dimensional devices based on quantum wells, quantum wires, and quantum dots, has prompted intense activity in the study of semiconductor heterostructures.[1–5] Nevertheless, spintronics is a new emerging field where the spin degree of freedom of electrons is used as a unit of information rather than its charge. This rapidly developing field aims to carry out controllable manipulations of electron spins with electric fields.[6] To comprehend the interaction between the particle's spin and its solid-state environment will open the possibility to design spintronic devices with higher speed and lower power consumption than of those currently existing.

Spin–orbit (SO) interaction in semiconductor heterostructures is an important tool for controlling the electron's spin.[7] Inversion asymmetry properties of low-dimensional systems lead to two basic mechanisms in SO interactions.[8,9] The lack of an inversion center in the crystal lattice in bulk semiconductors gives rise to the Dresselhaus SO[10] coupling whereas the asymmetric confining potential in the growth direction induces Rashba SO coupling.[11] Characteristic beating pattern in the magnetoresistance of a two-dimensional electron gas provides information on the SO coupling parameters.[12] Although the strengths of SO terms are difficult to measure independently, a full understanding of interplay between them is crucial for realizing spin-dependent phenomena in low-dimensional structures.[13]

External controllability of the transverse length of quantum wires (QWs) raises them to being appropriate structures for the development of spin-based devices.[6] In recent years, extensive studies have been carried out to investigate the electronic, spin, transport, and conductance properties of quasi-one-dimensional (1D) systems. A considerable amount of survey research has been performed on exhibiting the effects of SO interactions in the absence/presence of external fields.[14–18] Many theoretical and experimental works have searched electronic and transport properties of QWs taking into account Rashba SO interaction[19–25] and Dresselhaus SO interaction[9,16,26–31] under the influence of perpendicular magnetic fields. Despite that, lesser effort has been expended in exploring the effects of in-plane magnetic fields in QWs. Serra and coworkers[7] searched the spectral and transport properties of ballistic quasi-1D system under an in-plane magnetic field and Rashba SO interaction. Malet *et al.*[6] studied the effect of exchange correlation energy on the ground state structure of QW submitted on an in-plane magnetic field taking into account Rashba and Dresselhaus SO interactions. Tang *et al.*[32] investigated quantum transport in a narrow constriction fabricated by narrow-band-gap semi-conductor materials with SO couplings and in-plane magnetic field. Moreover, the optical properties of parabolically confined QW have been investigated under the influence of Rashba SO interaction and magnetic electric field by Khordad[33] and Lahon and coworkers.[34]

Although there are works related to the effects of Rashba and Dresselhaus SO interactions on the electronic structure and transport properties in quantum confined systems, to the best of our knowledge, spin textures in the local magnetization for parabolically confined QWs subjected to an in-plane magnetic field have not been studied. It is noteworthy to bring out the dependence of the spin texturing on the strength and orien-

†Corresponding author. E-mail: bircangisi@gmail.com

© 2016 Chinese Physical Society and IOP Publishing Ltd

tation of magnetic field and the magnitude of spin–orbit coupling, especially the Dreselhaus SO contribution. Even though many works reported the influence of the SO and magnetic field on the electronic structure, less attention has been paid to the spin texturing. Searching out the electrosubbands and spin density modulations could assist in understanding of transport and optical properties of quasi-1D quantum structures. In line with this purpose, in the present study, the investigation of competition effects between the SO interactions and in-plane magnetic field on energy subbands, spin expectation values, and spin textures of a parabolic QW has been carried out.

The organization of the rest of this paper is as follows. In Section 2, we briefly describe the system and present the methodology used throughout our study. In Section 3, we give the numerical results and discussion. A short concluding section (Section 4) summarizes our findings.

2. Model and method

We consider a quasi-1D quantum wire with a parabolic confinement in y-direction given as $V(y) = m^* \omega_0^2 y^2/2$ and correspondingly the wire orientation along x-direction as shown in Fig. 1. In-plane magnetic field applied with an arbitrary orientation is chosen as $\boldsymbol{B} = B(\cos\theta\, \boldsymbol{e}_x + \sin\theta\, \boldsymbol{e}_y)$ where θ represents an azimuthal angle.

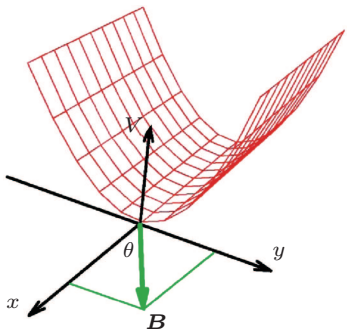


Fig. 1. (color online) The model of the quantum wire structure and the orientation of magnetic field.

Translational invariance along the x-direction allows us to write the wave function as a product of plane waves and y-dependent spinor part as follows:

$$\psi_{nk_x}(\boldsymbol{r}) = \frac{\mathrm{e}^{\mathrm{i}k_x x}}{\sqrt{L}} \begin{pmatrix} \varphi_{nk_x}(y,\uparrow) \\ \varphi_{nk_x}(y,\downarrow) \end{pmatrix}, \tag{1}$$

with φ_{nk_x} being the spinor function, we introduce a continuous wave number k_x, which is a good quantum number, and index of integer numbers $n = 1,2,3,\ldots$, labeling different energy subbands. By following a similar strategy to the one in Ref. [6], we use the finite-T frame formalism as a numerical trick, but results of actual calculations are for $T = 0$ case. Accordingly, the electron density can be written as

$$\rho(y) = \sum_n \frac{1}{2\pi} \int \mathrm{d}k_x (|\varphi_{nk_x}(y,\uparrow)|^2 + |\varphi_{nk_x}(y,\downarrow)|^2) f_\beta(\varepsilon_{nk_x}), \tag{2}$$

where $f_\beta(\varepsilon_{nk_x})$ is the Fermi function. Then, the one-dimensional electron density along the QW is $\rho_{1\mathrm{D}} = \int \mathrm{d}y \rho(y)$. The $\sigma_a (a = x,y,z)$ being the corresponding Pauli matrix, we can calculate spin magnetization components

$$m_a(y) = \sum_n \frac{L}{2\pi} \int \mathrm{d}k \langle \psi_{nk} | \delta(r_i - r) \sigma_a | \psi_{nk} \rangle_{r_i} f_\beta(\varepsilon_{nk}, \mu). \tag{3}$$

The single-particle Hamiltonian of the quasi-1D wire system is given by

$$\mathcal{H} = \mathcal{H}_0 + \mathcal{H}_\mathrm{Z} + \mathcal{H}_\mathrm{R} + \mathcal{H}_\mathrm{D}. \tag{4}$$

The first term $\mathcal{H}_0$, consists of the kinetic and confinement potential whereas the second term describes the Zeeman effect contribution arising from an in-plane magnetic field that are given explicitly

$$\mathcal{H}_0 = \frac{p_x^2 + p_y^2}{2m^*} + \frac{1}{2} m^* \omega_0^2 y^2, \tag{5}$$

$$\mathcal{H}_\mathrm{Z} = g^* \mu_\mathrm{B} B (\cos\theta \sigma_x + \sin\theta \sigma_y)/2. \tag{6}$$

In the above expressions, p_x and p_y are the actual components of linear momentum, m^* is the effective mass, ω_0 is oscillator frequency, g^* and μ_B are the effective Lande-g factor and Bohr magneton, respectively, σ_x and σ_y represent the Pauli spin matrix components.

The last two terms in Eq. (4) are spin–orbit contributions where Rashba Hamiltonian $(\mathcal{H}_\mathrm{R})$ is given as

$$\mathcal{H}_\mathrm{R} = \frac{\alpha_\mathrm{R}}{\hbar} (p_y \sigma_x - p_x \sigma_y), \tag{7}$$

and Dresselhaus Hamiltonian $(\mathcal{H}_\mathrm{D})$ is

$$\mathcal{H}_\mathrm{D} = \frac{\alpha_\mathrm{D}}{\hbar} (p_x \sigma_x - p_y \sigma_y). \tag{8}$$

Here, α_R and α_D stand for Rashba and Dresselhaus SO coupling parameters, respectively.[6,7] In 2D systems, Dresselhaus SO coupling term has two components, one is linear in the electron momentum and the other is cubic.[35] The cubic Dresselhaus term is generally ignored because its contribution is smaller than the linear one as stated in Refs. [31] and [36]. In our study, we ignore the cubic Dresselhaus spin–orbit contribution.

By introducing a complex SO coupling parameter $\gamma \equiv \alpha_\mathrm{D} + \mathrm{i}\alpha_\mathrm{R}$, taking into account the translational invariance along the x-direction and defining Zeeman energy $\varepsilon_z = (1/2) g^* \mu_\mathrm{B} B$, we obtain the eigenvalue equation in the form as follows:

$$\begin{pmatrix} -\frac{\hbar^2}{2m^*}\frac{\mathrm{d}^2}{\mathrm{d}y^2}+\frac{\hbar^2k_x^2}{2m^*}+\frac{1}{2}m^*\omega_0^2y^2 & \gamma^*\frac{\mathrm{d}}{\mathrm{d}y}+\gamma k_x+\varepsilon_z\mathrm{e}^{-\mathrm{i}\theta} \\ -\gamma\frac{\mathrm{d}}{\mathrm{d}y}+\gamma^*k_x+\varepsilon_z\mathrm{e}^{\mathrm{i}\theta} & -\frac{\hbar^2}{2m^*}\frac{\mathrm{d}^2}{\mathrm{d}y^2}+\frac{\hbar^2k_x^2}{2m^*}+\frac{1}{2}m^*\omega_0^2y^2 \end{pmatrix} \begin{pmatrix} \varphi_{nk_x\uparrow} \\ \varphi_{nk_x\downarrow} \end{pmatrix} = \varepsilon_{nk_x} \begin{pmatrix} \varphi_{nk_x\uparrow} \\ \varphi_{nk_x\downarrow} \end{pmatrix}, \tag{9}$$

where ε_{nk_x} are single-electron energies.

The numerical solution of Eq. (9) has been carried out with the finite element method based on Galerkian procedure.[37,38]

3. Results

In this study, we have investigated the electronic band structure and spin texturing of QW formed by a parabolic confining potential on the GaAs heterostructure with corresponding bulk parameters: $g^* = -0.44$, $m^* = 0.067m_0$, and dielectric constant $\varepsilon_r = 12.4$. The harmonic oscillator length $l_0 = \sqrt{\hbar/m^*\omega_0}$ is used as a length scale and the energies are scaled in $\hbar\omega_0$ units. We set $\hbar\omega_0$ to 2 meV which is a typical energy value for GaAs system.[39] Throughout this work, we use $\rho_{1\mathrm{D}}l_0 = 0.78$ as dimensionless electron density that corresponds to a linear density of 3.27×10^5 cm^{-1}. Considering the corresponding length associated with the Rashba (Dresselhaus) SO coupling strength ($l_{\mathrm{so}}^{\mathrm{R(D)}} = \hbar^2/2m^*\alpha_{\mathrm{R(D)}}$),[7] we can distinguish SO interactions into two regimes: weak regime when $l_0 \ll l_{\mathrm{so}}$ and strong regime when $l_0 \geqslant l_{\mathrm{so}}$. In the present work characterization of the SO regime is realized by the ratio of the strength of SO interaction to the confinement potential energy, $\Delta_{\mathrm{R(D)}} = m^*\alpha_{\mathrm{R(D)}}^2/2\hbar^3\omega_0$. For GaAs/AlGaAs structure SO coupling constants are experimentally of the order of 10^{-11} eV·m.[15,40,41] By virtue of this fact, parameters $\Delta_{\mathrm{R(D)}} \gtrsim 0.1$ define the strong SO and $\Delta_{\mathrm{R(D)}} < 0.1$ account for the weak SO regime.[26]

Initially, in order to identify how the interplay between Rashba and Dresselhaus SO coupling affects the energy subband structure of quantum wire, in Figs. 2(a)–2(c) we give E–k graphs for different strengths of SO contributions in the absence of magnetic field. It is well known that, in the absence of a magnetic field and SO interaction, spin-up and spin-down states within each subband are degenerate for all values of k_xl_0. Taking into account Rashba SO interaction leads to spin-splitting except the point $k_xl_0 = 0$ while manifesting itself as two laterally displaced parabolas. With the further increment in Rashba SO interaction, the degeneracy is preserved only for eigenstates with $k_x = 0$ and coupling between spin-split levels appears.[7,20,24,25,27,42] Switching on the Dresselhaus term in the Hamiltonian brings out more pronounced anticrossings, especially at higher levels, even for weak strengths of Dresselhaus SO coupling. In the Fig. 2(a), the energy subband for

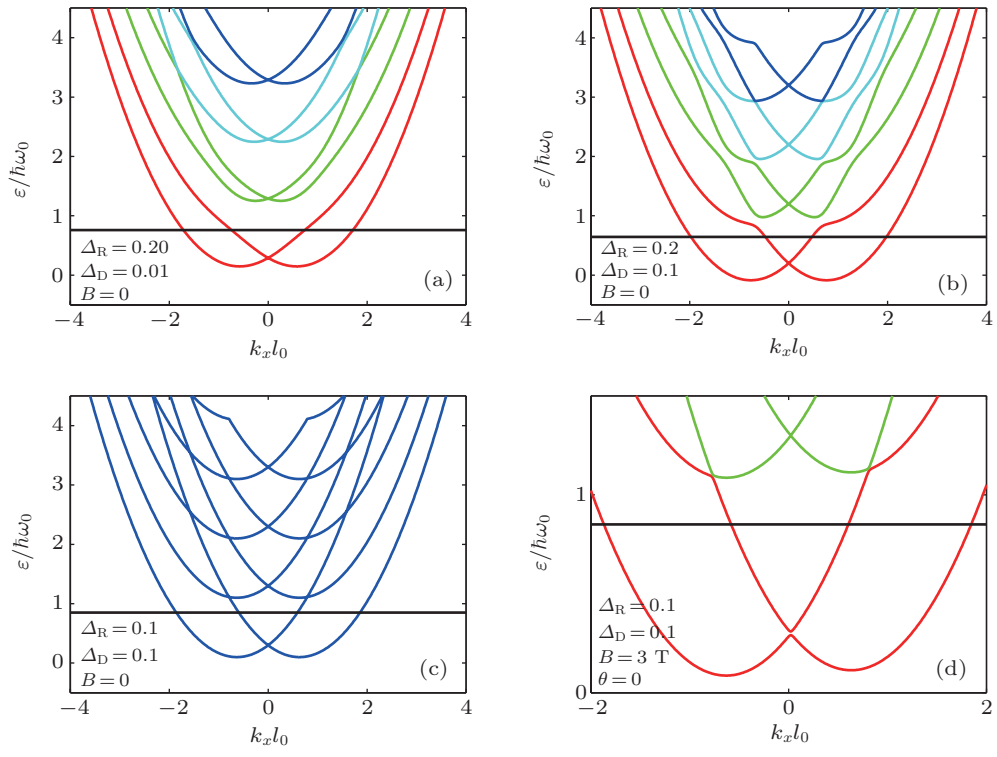


Fig. 2. (color online) Subband energy spectra as a function of linear momentum k_xl_0. Here, (a) $\Delta_{\mathrm{R}} = 0.2$ and $\Delta_{\mathrm{D}} = 0.01$, and (b) $\Delta_{\mathrm{R}} = 0.2$ and $\Delta_{\mathrm{D}} = 0.1$, (c) $\Delta_{\mathrm{R}} = \Delta_{\mathrm{D}} = 0.1$ for zero external magnetic field. (d) In the presence of external magnetic field of 3 T applied parallel to the wire-axis for $\Delta_{\mathrm{R}} = 0.1$ and $\Delta_{\mathrm{D}} = 0.1$. The thin horizontal line indicates the chemical potential for the linear density $\rho_{1\mathrm{D}}l_0 = 0.78$.

the case of strong Rashba SO interaction ($\Delta_R = 0.2$) and weak Dresselhaus SO interaction ($\Delta_D = 0.01$) is presented. Nearly parabolic structure and subband coupling in higher levels leap out. Simultaneous contribution of both SO interaction terms in strong regime ($\Delta_R = 0.2$ and $\Delta_D = 0.1$) results in stronger deviation from parabolicity of the subbands and downward shifting of energy. As seen in Fig. 2(b) more complex subband structure and more pronounced anticrossings comprise between subbands of different levels in the vicinity of $k_x = 0$ in comparison with the previous case (Fig. 2(a)). Unique feature comes up in a particular situation for equal strengths of Rashba and Dresselhaus SO interactions in zero magnetic field case. Parabolic energy dispersions with no avoided crossings[43] can be seen in Fig. 2(c). To elucidate the interplay between SO interaction and magnetic field, in Fig. 2(d) we show the energy subband structure for characteristic SO energies $\Delta_R = \Delta_D = 0.1$ at magnetic field of 3 T orientated along the wire axis. The zero-field crossing point becomes an anticrossing, called a spin–orbit gap,[15] and the first subband presents double minimum structure that plays an important role in the explanation of anomalous steps in the conductance.

Next, we want to illustrate dependence of the spin–orbit gap on the strength of Dresselhaus SO interaction. In Fig. 3(a) we present the lowest and first-excited spin-split subband of a quantum wire subjected to magnetic field of 5 T oriented along the wire confinement for a fixed strength of Rashba SO interaction ($\Delta_R = 0.05$). In the case of a weak regime where both SO couplings are small, asymmetric double minimum structure in the odd spin-split subbands is visible. Increment in Δ_D results in a downward energy shift at degeneracy point $k_x = 0$. Moreover, for the even energy levels a local extremum in the vicinity of $k_x = 0$ comes up. Note that due to the combined effect of increasing Dresselhaus SO interaction and in-plane magnetic field the k-splitting increases nearly linearly with Δ_D.

Dependence of the energy subbands on the orientation of the magnetic field is considered in Fig. 3(b). We assume that the wire is under the influence of external magnetic field of 5 T applied along different directions. SO coupling parameters are chosen as $\Delta_R = 0.2$ and $\Delta_D = 0.1$ and solid, dashed, and dotted lines in the figure correspond to $\theta = 0, \pi/4, \pi/2$, respectively. Combined effect of SO interaction and magnetic field removes degeneracies at all k_x independently of the direction of magnetic field.[6,9,26] In Ref. [1] where only Rashba SO coupling is taken into account, it has been reported that a gap between two spin-split bands appears at $k_x = 0$ only in the case of $\theta = 0$ or $\theta = \pi/4$. In the present study we observe the subband gap for all orientations of magnetic field. Magnetic field induces k-asymmetries in the subband energy spectra. When the field is chosen along the wire axis ($\theta = 0$) the minimum energy point is observed at negative k_x values, whereas for $\theta = \pi/2$ this minimum shifts to positive k_x. We note that when the field is oriented with an angle $\theta = \pi/4$, a symmetric double minimum energy structure is observed.

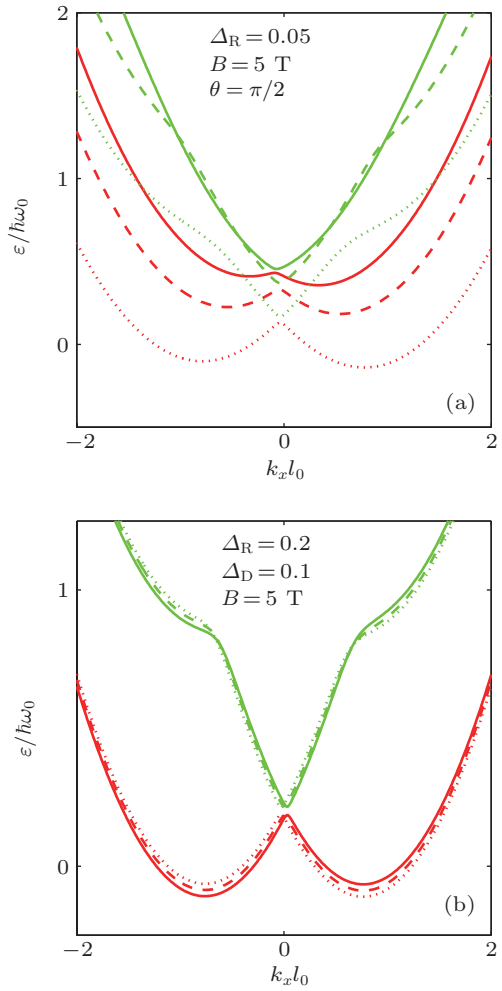


Fig. 3. (color online) Dispersion relations of the lowest subbands. (a) Variation of the energies for weak Rashba SO coupling $\Delta_R = 0.05$ and magnetic field $B = 5$ T described with an angle $\theta = \pi/2$. Solid line presents $\Delta_D = 0.01$, dashed line corresponds to $\Delta_D = 0.1$, and the dotted line stands for $\Delta_D = 0.3$. (b) Dependence of the first spin-split subband on the orientation of external magnetic field for strong SO regime characterized by $\Delta_R = 0.2$ and $\Delta_D = 0.1$. Solid line corresponds to $\theta = 0$, the dashed line presents $\theta = \pi/4$, and the dotted line is $\theta = \pi/2$.

When SO coupling is ignored, the states are exact eigenspinors even in the presence of in-plane magnetic field.[1] But whenever the typical SO interaction energy scale becomes comparable to the subband splitting, emergence of a sizable spin z-component due to anticrossings between neighboring subbands precludes a definition of common spin-quantization axis.[24] This situation results in occurrence of spin textures across the wire with the spin direction depending on k_x and the wire transversal coordinate y. In the following part of the study, we illustrate the effects of SO interaction and magnetic field on the modification of the spin orientation. In this respect, we calculated spin expectation values $\langle \sigma_n \rangle = \Psi_{nk}^{\dagger} \sigma_n \Psi_{nk}$, where $n = x, y, z$.[7]

In Fig. 4, we plot spin projections of eigenstates for the lowest spin-split subbands. For a fixed value of Rashba SO coupling ($\Delta_R = 0.05$) $k_x l_0$-dependence of $\langle\sigma_x\rangle$ and $\langle\sigma_y\rangle$ is investigated considering different strengths of Dresselhaus SO coupling. Preferred direction of magnetic field of 5 T is chosen along the wire axis. The local z-magnetization in real space $\langle\sigma_z(y)\rangle$ is antisymmetric in y and therefore integrated $\langle\sigma_z\rangle$ is equal to zero. In the presence of pure Rashba SO coupling (blue-dashed line) at $k_x l_0 = 0$ the value of $\langle\sigma_x\rangle$ is equal to a constant as seen in Fig. 4(a). Despite that, for larger values of k_x asymptotic eigenstates of σ_y are clearly seen in Fig. 4(b). With addition of Dresselhaus term, significant change in the behavior of $\langle\sigma_x\rangle$ is observed, even for a weak interaction regime. On the other hand, the general attitude of $\langle\sigma_y\rangle$ does not change remarkably. We also observe that stronger Dresselhaus SO contribution acts in an opposite manner on $\langle\sigma_x\rangle$ and $\langle\sigma_y\rangle$.

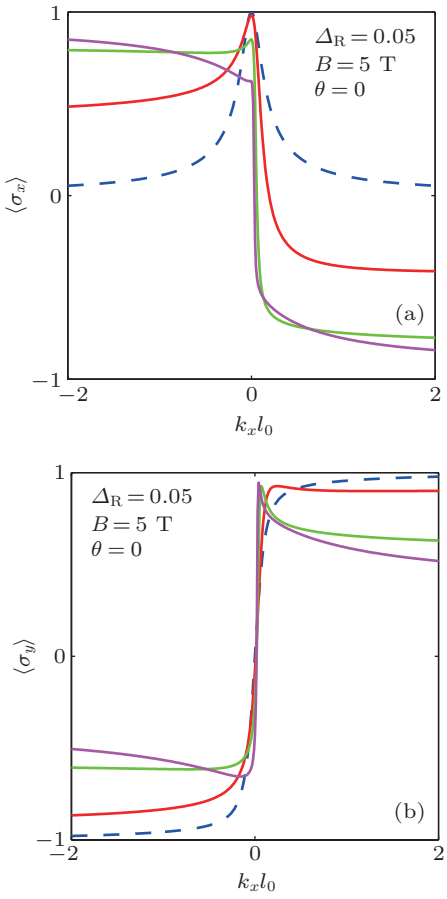


Fig. 4. (color online) Spin projections of eigenstates in the lowest spin-split subbands. (a) Variation of $\langle\sigma_x\rangle$ for different strengths of Dresselhaus SO coupling where red, green, and magenta lines corresponds to $\Delta_D = 0.01, 0.1, 0.3$, respectively. (b) The same as (a) but for $\langle\sigma_y\rangle$. In both figures the blue-dashed line presents the case of pure Rashba SO interaction.

We have investigated the local spin components for the lowest subband for the strong SO coupling regime characterized by $\Delta_R = 0.2$ and $\Delta_D = 0.1$ in the presence of magnetic field $B = 1$ T chosen along the wire orientation. In Figs. 5(a)–5(c), the local spin components at three different propagation momenta are presented. The vector plot shows the in-plane spin whereas the solid line corresponds to the z-component. As seen in Figs. 5(a) and 5(c), the local spin components present opposite spin accumulations at $k_x l_0 = -0.76$ and $k_x l_0 = 0.76$. At the point $k_x l_0 = 0$, the spin components have the maximum amplitude and almost all local spins are aligned along the direction of transport. In the presence of pure Rashba SO, the local z-component is equal to zero for $k_x l_0 = 0$,[7] but with an inclusion of Dresselhaus SO coupling, this component becomes different from zero. This can be interpreted as Dresselhaus SO interaction causes a rise in the spin component. We should note that considering weak Rashba SO coupling ($\Delta_R = 0.02$) when the other parameters are kept the same, the magnitude of spin components decreases. In Fig. 5(d), we plot the spin expectation values in the lowest subband where blue and red lines denote σ_x and σ_y, respectively. The dotted line represents the case with no SO interaction, the dashed line shows the pure Rashba SO interaction case and the solid line stands

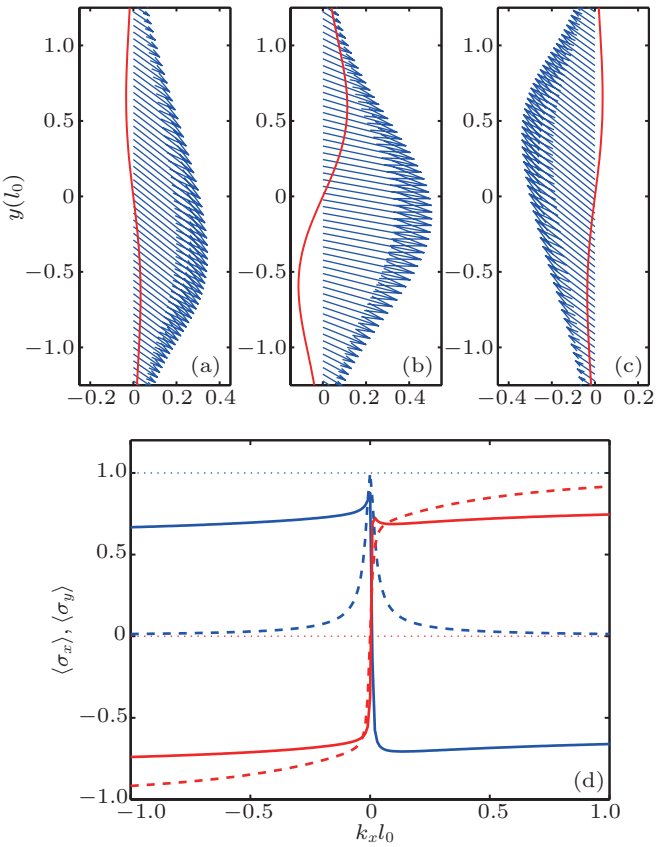


Fig. 5. (color online) Upper panels display the spin texture for three selected propagation momenta: Panels (a)–(c) correspond to $k_x l_0 = -0.76, 0, 0.76$, respectively where arrow length is proportional to the spin density. We set $\Delta_R = 0.2$ and $\Delta_D = 0.1$ and assume magnetic field of 1 T applied parallel to the wire. Lower panel (d) presents the dependence of spin expectation values in the lowest subband on $k_x l_0$. Blue lines indicate $\langle\sigma_x\rangle$ whereas red lines represent $\langle\sigma_y\rangle$. Dotted lines stand for the case with no SO interaction, dashed curves are for $\Delta_R = 0.2$ and $B = 1$ T case, and the results when both SO interactions taken into account are given by solid lines.

for the case in the presence of both SO interactions. It is clear that $\langle\sigma_x\rangle$ and $\langle\sigma_y\rangle$ are constant for all $k_x l_0$ considering only the influence of magnetic field. By inclusion of SO coupling the expectation values show variation with $k_x l_0$. In the presence of both a magnetic field and spin–orbit interactions, states with large k_x values approach to asymptotic states of $\langle\sigma_x\rangle$ and $\langle\sigma_y\rangle$. Intriguing spin textures arising due to the interplay between SO coupling and magnetic field have also been reported in mesoscopic ring systems.[44]

In Fig. 6, we plot spin textures across the wire and the spin expectation values for the second level of the lowest spin-split subband using the same parameters as in Fig. 5. The SO interaction is more notable than in the lowest subband as shown in upper panels. Spin textures contain a noncollinear distribution and the local z-magnetization is greater than the lowest subband. Its magnitude exceeds the in-plane components while giving rise to large spin accumulations at the wire edges. For the minimum gap point, all local spins are again aligned in the direction of transport. Lower panel in the figure reveals the remarkable change in the spin expectation values $\langle\sigma_x\rangle$ and $\langle\sigma_y\rangle$ for the second spin-split level. Subband anticrossings in the presence of both SO interactions evoke the smooth behavior of $\langle\sigma_x\rangle$ and $\langle\sigma_y\rangle$.

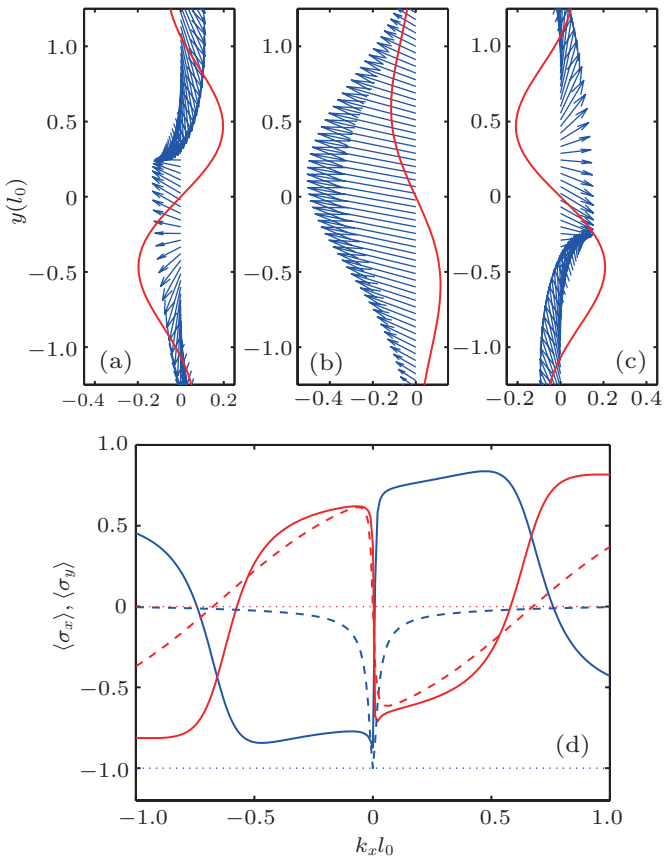


Fig. 6. (color online) The same as Fig. 5 for the second subband. Panels (a)–(c) display the spin texture for three selected propagation momenta and panel (d) presents the spin expectation values.

In order to clarify the relation between the spin expectation value and the orientation of magnetic field, in Fig. 7, we present the variations of $\langle\sigma_x\rangle$ and $\langle\sigma_y\rangle$ as a function of linear momentum $k_x l_0$. This chromatic scale reveals the fact that spin expectation values are opposite for left and right movers. For higher values of $k_x l_0$, monotonous variation of spin expectation values with increasing θ is evident.

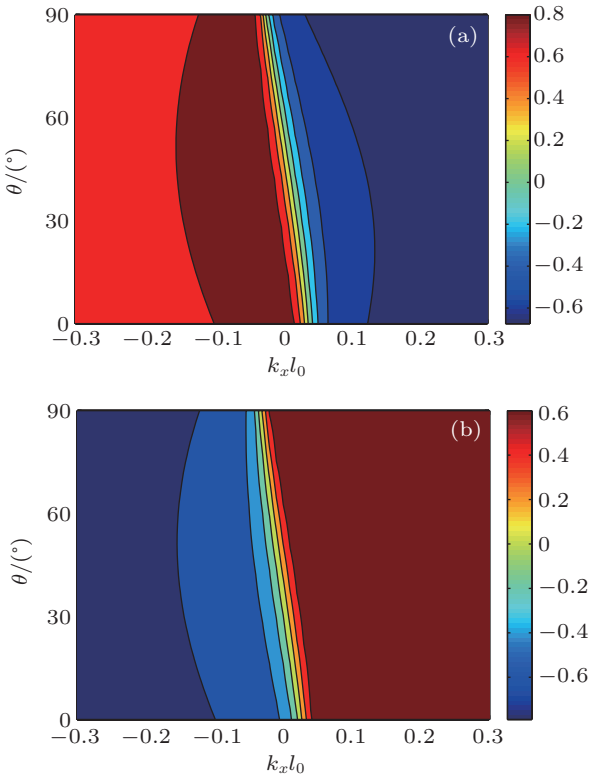


Fig. 7. (color online) The expectation values of σ_x (a) and σ_y (b) in chromatic scale for strong SO regime defined by $\Delta_R = 0.2$, $\Delta_D = 0.1$. We chose magnetic field of $B = 5$ T. The color bar indicates values of expectation value of the spin projections.

4. Conclusion

In this study, we have investigated the energy subband structure and spin texturing of quantum wire in the presence of Rashba and Dresselhaus SO interactions and in-plane magnetic fields. We have found that, the interplay between the SO coupling and magnetic field affects strongly the energy dispersion of the wire. Our numerical calculations show that the spin textures in the local magnetization can be modulated by SO interactions as well as the orientation and the magnitude of the external magnetic field. We expect that these results can assist in understanding the crucial role of Rashba and Dresselhaus couplings for the spin injection across realistic quasi-one-dimensional systems.

Acknowledgment

One of the authors (B Gisi) would like to thank the Scientific and Technological Research Council of Turkey

(TUBITAK BIDEB 2210 program) for support of a scholarship.

References

[1] Pershin Y V, Nesteroff J A and Privman V 2004 *Phys. Rev. B* **69** 121306
[2] Perroni C A, Bercioux D, Ramaglia C A and Cataudella V 2007 *J. Phys.: Condens. Mattter* **19** 186227
[3] Kelly M J 1995 *Low Dimensional Semiconductors: Materials, Physics, Technology, Devices* (Oxford: Oxford University Press)
[4] Mireles F K G 2001 *Phys. Rev. B* **64** 024426
[5] Wang Y, Djie H S, Ooi B S, Rotella P, Dowd P, Aimez V, Cao Y and Zhang Y H 2007 *Thin Solid Films* **515** 4352
[6] Malet F, Pi M, Barranco M, Serra L and Lipparini E 2007 *Phys. Rev. B* **76** 115306
[7] Serra L, Sánchez D and López R 2005 *Phys. Rev. B* **72** 235309
[8] Winkler R 2003 *Spin–Orbit Coupling Effects in Two-Dimensional Electron and Hole Systems* (Berlin: Springer)
[9] Zhang T Y, Zhao W and Liu M 2009 *J. Phys.: Condens. Matter* **21** 335501
[10] Dresselhaus G 1955 *Phys. Rev.* **100** 580
[11] Rashba E I 1960 *Sov. Phys. Solid. State* **2** 1109
[12] Guzenko V A, Knobbe J, Hardtdegen H and Schäpers Th 2006 *Appl. Phys. Lett.* **88** 032102
[13] Krich J J and Halperin B I 2007 *Phys. Rev. Lett.* **98** 226802
[14] Canham L T 1990 *Appl. Phys. Lett.* **57** 1046
[15] Guay C H L, Hýghes T L, Sulpizio J A, Pfeiffer L N, Baldwin K W, West K W, Goldhaber-Gordon D and de Picciatto R 2010 *Nat. Phys.* **6** 336
[16] Gujarathi S, Alam K M and Pramanik S 2012 *Phys. Rev. B* **85** 045413
[17] Orellana P A, Dominguez-Adame F, Gomez I and de Guevara M L L 2003 *Phys. Rev. B* **67** 085321
[18] Abonov A 2012 *Phys. Rev. B* **85** 085311
[19] Schäpers Th, Knobbe J and Guzenko V A 2004 *Phys. Rev. B* **69** 235323
[20] Knobbe J and Schäpers Th 2005 *Phys. Rev. B* **71** 035311
[21] Debald S and Kramer B 2005 *Phys. Rev. B* **71** 115322
[22] de Andrade e Silva E A and La Rocaa G C 2003 *Phys. Rev. B* **67** 165318
[23] Erlingson S J, Egues J C and Loss D 2006 *Phys. Status Solidi A* **3** 4317
[24] Governale M and Zülicke U 2002 *Phys. Rev. B* **66** 073311
[25] Governale M and Zülicke U 2004 *Solid State Commun.* **131** 581
[26] Zhang S, Liang R, Zhang E, Zhang L and Liu Y 2006 *Phys. Rev. B* **73** 155316
[27] Moroz A V and Barnes C H W 2000 *Phys. Rev. B* **61** R2464
[28] Pramanik S, Bandyopadhyay S and Cahay M 2007 *Phys. Rev. B* **76** 155325
[29] Upadhyaya P, Pramanik S, Bandyopadhyay S and Cahay M 2008 *Phys. Rev. B* **77** 045306
[30] Upadhyaya P, Pramanik S and Bandyopadhyay S 2008 *Phys. Rev. B* **77** 155439
[31] Sarikurt S, Sakiroglu S, Akgungor K and Sokmen I 2014 *Chin. Phys. B* **23** 017102
[32] Tang C S, Chang S Y and Cheng J 2012 *Phys. Rev. B* **86** 125321
[33] Khordad R 2013 *J. Lumin.* **134** 201
[34] Lahon S, Kumar M, Jha P K and Mohan M 2013 *J. Lumin.* **144** 149
[35] Yang W and Chang K 2006 *Phys. Rev. B* **74** 193314
[36] Krich J J and Halperin B I 2007 *Phys. Rev. Lett.* **98** 226802
[37] Zienkiewicz O C, Taylor R L and Zhu J Z 2005 *The Finite Element Method: Its Basis and Fundamentals (5th edn.)* (Planta Tree)
[38] Pask J E, Klein B M, Sterne P A and Fong C Y 2001 *Comput. Phys. Commun.* **135** 1
[39] Wang C, Wang H and Zhang Q 1999 *Chin. Phys. Lett.* **16** 373
[40] Miller J B, Zumbühl D M, Marcus C M, Lyanda-Geller Y B, Goldhaber-Gordon D, Campman K and Gossard A C 2003 *Phys. Rev. Lett.* **90** 076807
[41] Könemann J, Haug R J, Maude D K, Falko V I and Altshuler B L 2007 *Phys. Rev. Lett.* **94** 226404
[42] Moroz A V and Barnes C H W 1999 *Phys. Rev. B* **60** 14272
[43] Schliemann J, Egues J C and Loss D 2003 *Phys. Rev. Lett.* **90** 146801
[44] Sheng J S and Chang K 2006 *Phys. Rev. B* **74** 235315